Vector diffraction analysis of high numerical aperture focused beams modified by two- and three-zone annular multi-phase plates

Toufic G. Jabbour[1] and Stephen M. Kuebler[1, 2]

[1]College of Optics and Photonics: CREOL & FPCE
[2]Department of Chemistry
University of Central Florida, Orlando, FL, USA 32816
mailto:kuebler@mail.ucf.edu

Abstract: Vector diffraction theory was applied to study the effect of two- and three-zone annular multi-phase plates (AMPs) on the three-dimensional point-spread-function (PSF) that results when linearly polarized light is focused using a high numerical aperture refractory lens. Conditions are identified for which a three-zone AMP generates a PSF that is axially super-resolved by 19% with minimal change in the transverse profile and sufficiently small side lobes that the intensity pattern could be used for advanced photolithographic techniques, such as multi-photon 3D microfabrication, as well as multi-photon imaging. Conditions are also found in which a three-zone AMP generates a PSF that is axially elongated by 510% with only 1% change along the transverse direction. This intensity distribution could be used for sub-micron-scale laser drilling and machining.

OCIS codes: (100.6640) Superresolution; (050.1220) Apertures; (170.5810) Scanning microscopy.

References and links

1. S. F. Pereira and A. S. van de Nes, "Superresolution by means of polarization, phase and amplitude pupil masks," Opt. Commun. **234**, 119-124 (2004).
2. A. Diaspro, *Confocal and Two-Photon Microscopy: Foundations, Applications, and Advances* (Wiley, New York, 2002).
3. T. R. M. Sales and G. M. Morris, "Diffractive superresolution elements," J. Opt. Soc. Am. A **14**, 1637-1646 (1997).
4. T. R. M. Sales and G. M. Morris, "Axial superresolution with phase-only pupil filters," Opt. Commun. **156**, 227-230 (1998).
5. X.-F. Zhao, C.-F. Li and H. Ruan, "Improvement of three-dimensional resolution in optical data storage by combination of two annular binary phase filters," Chin. Phys. Lett. **21**, 1515-1517 (2004).
6. S. Zhou and C. Zhou, "Discrete continuous-phase superresolving filters," Opt. Lett. **29**, 2746-2748 (2004).
7. H. Wang and F. Gan, "High focal depth with pure-phase apodizer," Appl. Opt. **40**, 5658-5662 (2001).
8. H. Y. Chen, N. Mayhew, E. G. S. Paige and G. G. Yang, "Design of the point spread function of a lens, binary phase filter combination and its application to photolithography," Opt. Commun. **119**, 381-389 (1995).
9. G. Yang, "An optical pickup using a diffractive optical element for a high-density optical disc," Opt. Commun. **159**, 19-22 (1999).
10. C. Ibáñez-López, G. Saavedra, G. Boyer and M. Martínez-Corral, "Quasi-isotropic 3-D resolution in two-photon scanning microscopy," Opt. Express **13**, 6168-6174 (2005).
11. C. Ibáñez-López, G. Saavedra, K. Plamann, G. Boyer and M. Martínez-Corral, "Quasi-spherical focal spot in two-photon scanning microscopy by three-ring apodization," Microsc. Res. Tech. **67**, 22-26 (2005).
12. B. Kress and P. Meyrueis, *Digital Diffractive Optics* (Wiley, New York, 2000).
13. H. Ando, "Phase-shifting apodizer of three or more portions," Jap. J. Appl. Phys. **31**, 557-567 (1992).
14. M. P. Cagigal, J. E. Oti, V. F. Canales and P. J. Valle, "Analytical design of superresolving phase filters," Opt. Commun. **241**, 249-253 (2004).
15. V. F. Canales, J. E. Oti and M. P. Cagigal, "Three-dimensional control of the focal light intensity distribution by analytically designed phase masks," Opt. Commun. **247**, 11-18 (2005).
16. D. M. de Juana, J. E. Oti, V. F. Canales and M. P. Cagigal, "Design of superresolving continous phase filters," Opt. Lett. **28**, 607-609 (2003).

#10013 - $15.00 USD Received 19 December 2005; revised 21 January 2006; accepted 23 January 2006

17. M. Martínez-Corral, P. Andrés, J. Ojeda-Castañeda and G. Saavedra, "Tunable axial superresolution by annular binary filters. Application to confocal microscopy," Opt. Commun. **119**, 491-498 (1995).
18. M. Martínez-Corral, P. Andrés, C. J. Zapata-Rodríguez and M. Kowalczyk, "Three-dimensional superresolution by annular binary filters," Opt. Commun. **165**, 267-278 (1999).
19. M. Martínez-Corral, M. T. Caballero, E. H. K. Stelzer and J. Swoger, "Tailoring the axial shape of the point spread function using the Toraldo concept," Opt. Express **10**, 98-103 (2002).
20. S. Ching-Cherng and L. Chin-Ku, "Ultrasmall focusing spot with a long depth of focus based on polarization and phase modulation," Opt. Lett. **28**, 99-101 (2003).
21. M. Martínez-Corral, C. Ibáñez-López, G. Saavedra and M. T. Caballero, "Axial gain resolution in optical sectioning fluorescence microscopy by shaded-ring filters," Opt. Express **11**, 1740-1745 (2003).
22. M. Martínez-Corral, R. Martinez-Cuenca, I. Escobar and G. Saavedra, "Reduction of focus size in tightly focused linearly polarized beams," Appl. Phys. Lett. **85**, 4319-4321 (2004).
23. C. J. R. Sheppard and A. Choudhury, "Annular pupils, radial polarization, and superresolution," Appl. Opt. **43**, 4322-4327 (2004).
24. E. Wolf, "Electromagnetic diffraction in optical systems I. An integral representation of the image field," Proc. Royal Soc. A **253**, 349-357 (1959).
25. B. Richards and E. Wolf, "Electromagnetic diffraction in optical systems II. Structure of the image field in an aplanatic system," Proc. Royal Soc. A **253**, 358-379 (1959).
26. J. J. Stamnes, *Waves in Focal Regions: Propagation, Diffraction and Focusing of Light, Sound and Water Waves*, in *The Adam Hilger Series on Optics and Optoelectronics*, E. R. Pike and W. T. Welford, eds., (Adam Hilger, Bristol, 1986).
27. H. Liu, Y. Yan, D. Yi and G. Jin, "Design of three-dimensional superresolution filters and limits of axial optical superresolution," Applied Optics **42**, 1463-1476 (2003).
28. S. M. Kuebler and M. Rumi, "Nonlinear optics -- applications: three-dimensional microfabrication," in *Encyclopedia of Modern Optics*, R. D. Guenther, D. G. Steel and L. Bayvel, eds. (Elsevier, Oxford, 2004).
29. S. M. Kuebler, M. Rumi, T. Watanabe, K. Braun, B. H. Cumpston, A. A. Heikal, L. L. Erskine, S. Thayumanavan, S. Barlow, S. R. Marder and J. W. Perry, "Optimizing two-photon initiators and exposure conditions for three-dimensional lithographic microfabrication," J. Photopolym. Sci. Technol. **14**, 657-668 (2001).
30. H.-B. Sun, K. Takada, M.-S. Kim, K.-S. Lee and S. Kawata, "Scaling laws of voxels in two-photon photopolymerization nanofabrication," Appl. Phys. Lett. **83**, 1104-1106 (2003).
31. C. J. R. Sheppard and Z. S. Hegedus, "Axial behavior of pupil-plane filters," J. Opt. Soc. Am. A **5**, 643-647 (1988).

1. Introduction

Performance can be improved in many optical applications by engineering the focused three-dimensional (3D) intensity distribution, or point-spread-function (PSF), using diffractive optical elements (DOEs). DOEs are passive components that can be placed in the pupil plane of an optical system to alter the amplitude, phase, and polarization of the light prior to focusing [1]. The resolution achieved in scanned-laser imaging techniques, such as confocal and multi-photon microscopy, is determined by the transverse and axial extent of the central (most intense) lobe of the diffraction-limited PSF [2]. DOE designs have been reported that can decrease the lateral or axial extent of the central lobe, and this is frequently referred to as super-resolving [3-6]. In other applications it is beneficial to elongate the PSF axially so the focused intensity remains peaked over a greater depth of field [7,8] This enables uniform laser cutting of topographically complex work pieces, such as corrugated steel, and improved signal-to-noise in some optical data storage and read-out schemes [9].

DOE design and performance have been examined computationally and experimentally [10,11]. Radially symmetric amplitude-only and phase-only DOEs have attracted the most attention because they are structurally simple and relatively easy to fabricate using commonly available manufacturing and replication techniques [12]. Rotationally symmetric phase-only DOEs, or annular multi-phase plates (AMPs, Fig. 1), offer a significant advantage over amplitude-only DOEs in that they can deliver a greater fraction of incident optical power to the sample.

Computational approaches involving various levels of approximation have been applied to study how AMPs affect the PSF in the vicinity of the focus. Most investigations employ the scalar, paraxial approximation [13-19]. Scalar approaches are mainly based on the Fresnel model of diffraction. In some reports the second-order approximation of the focal intensity distribution was used to derive analytical expressions for the AMP-modified PSF [15]. These

#10013 - $15.00 USD Received 19 December 2005; revised 21 January 2006; accepted 23 January 2006

approximations greatly decrease computation time, but forfeit information concerning the vector character of the field. It is well known that under high numerical aperture (*NA*) conditions, rays refracted near the periphery of the limiting aperture have a non-zero longitudinal field component (component parallel to the direction of propagation). This contribution to the overall intensity distribution is unaccounted for in scalar methods, so they do not accurately model focusing and DOE performance in a high-*NA* configuration. A detailed analysis of binary- and multi-phase annular filters in the scalar limit has been reported by Sales and Morris [3].

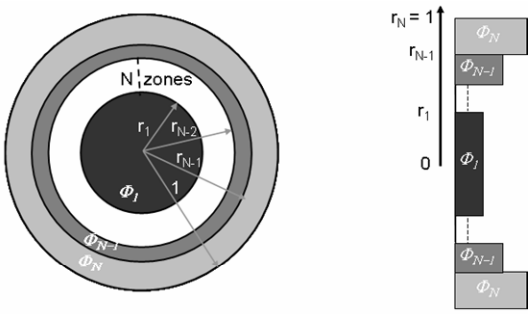

Fig. 1. Front (left) and profile (right) views of an annular multi-phase plate (AMP). The parameters Φ_i and r_i represent the differential phase transmittance and fractional radius of the *i*th annular zone, respectively.

Accurate modeling of high-*NA* focusing can be achieved using vector diffraction theory [1,20-23], which is equally well known as electromagnetic diffraction theory. The vector diffraction integrals derived by Wolf [24], and later extended to radially symmetric systems by Richards and Wolf [25], provide a means for directly computing the intensity distribution around the focus for an optical system that includes a phase aberration. Vector diffraction methods have been employed to examine some specific DOE configurations. Sheppard *et al*. applied this method to study how an amplitude DOE alters the transverse intensity distribution [23]. Martínez-Corral *et al*. used the vector diffraction method to study axial super-resolution achieved using amplitude-only DOEs [22].

The AMP-modified PSF has commonly been regarded as super-resolved in the axial/transverse direction if the separation between local minima adjacent to the primary lobe is decreased relative to that of the diffraction limited intensity distribution. Particularly in studies using vector diffraction methods, little attention has been paid to changes in the relative intensities of the main lobe and adjacent side lobes. It is known that AMPs alter the PSF such that the intensities of side lobes and local minima adjacent to the central lobe can become large and non-negligible in many applications. This is particularly true when the photo-response depends upon an absolute threshold intensity, as is the case for photolithographic techniques. Thus, more complete knowledge of the full 3D-PSF is required before a particular AMP design can be regarded as useful for a given application.

In this work, the Richard-Wolf integrals are applied to evaluate the entire solutions space of two- and three-zone AMPs and their effect on the PSF generated under high-*NA* refractive focusing. Emphasis is placed on characterizing changes in the axial extent of the central lobe and changes in the relative intensity of side lobes. These characteristics are most relevant to multi-photon imaging techniques, multi-photon 3D microfabrication, and optical data storage and read-out schemes.

2. Method and theory

Richards and Wolf formulated an integral representation of the electromagnetic field formed in the image space of an aplanatic optical system that images a point source located at infinity in the object space [24]. This theory is well suited for modeling the effect of AMPs on the focused PSF under high-*NA* conditions. The optical geometry is depicted in Fig. 2. An *N*-

#10013 - $15.00 USD Received 19 December 2005; revised 21 January 2006; accepted 23 January 2006

zone AMP and an aberration free lens (or lens system) are positioned such that their optical axes are collinear with the *z*-axis of a cylindrical coordinate system whose origin is located at the Gaussian focus of the lens. The numerical aperture is *NA* = 1.4 in all calculations, unless otherwise stated. Monochromatic linearly polarized plane waves, with electric field vector parallel to the *x*-axis, propagate along the *z*-axis, passing through the AMP and entering the pupil of the lens. The light focuses into a medium of refractive index $n = 1.5$. In the absence of the AMP, the situation is consistent with common applications of high-*NA* oil-immersion objective lenses.

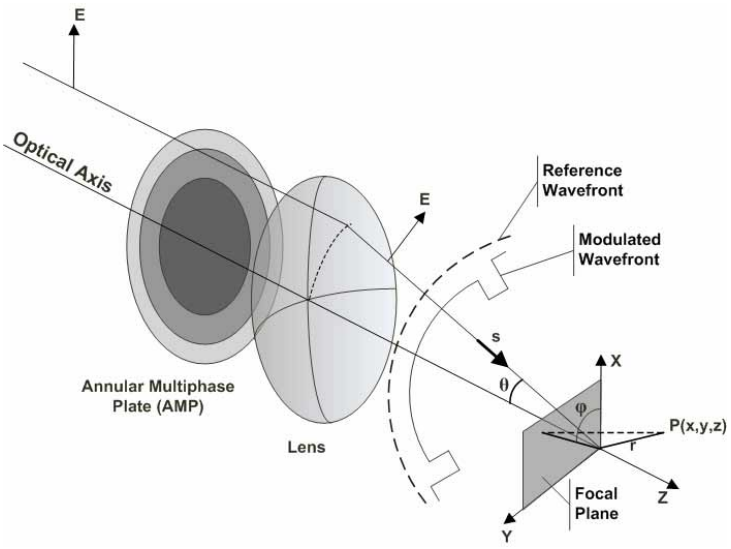

Fig. 2. Optical geometry in which an AMP is used to modify the phase front and resulting PSF of a focused optical beam.

The electric field at point $P(x, y, z)$ in the neighborhood of the focus may be expressed in the cylindrical optical coordinate system $[u, v, \varphi]$ as

$$\begin{aligned} e_x(u,v,\varphi) &= -iA(I_0 + I_2 \cos 2\varphi) \\ e_y(u,v,\varphi) &= -iAI_2 \sin 2\varphi \\ e_z(u,v,\varphi) &= -2AI_1 \cos\varphi \end{aligned} \tag{1}$$

The intensity at P is $I \propto |e_x + e_y + e_z|^2$, and the PSF is a spatial map of intensity for all values of $[u, v, \varphi]$ about the focus. φ is defined as the angle subtended by the electric field vector of the incident field and the meridional plane in which the field is calculated. The constant $A = \pi l_0 f/\lambda$ is defined in terms of the focal length, f, the wavelength within the medium, λ, and l_o, which describes the amplitude distribution of the incident field. It is assumed that uniform amplitude plane waves impinge on the lens, so l_o is set to unity.

Equation (1) is expressed in terms of the cylindrical optical coordinates u and v:

$$\begin{aligned} u &= kz \sin^2 \alpha \\ v &= kr \sin \alpha \end{aligned} \tag{2}$$

where z and r are the radial and axial coordinates, respectively, of the point in the original coordinate system. The maximum aperture angle, $\alpha = \arcsin(NA/n)$, is determined by the numerical aperture of the lens. The wave number $k = 2\pi/\lambda$. $I_{0,1,2}$ are integrals evaluated over the aperture half-angle θ as

#10013 - $15.00 USD Received 19 December 2005; revised 21 January 2006; accepted 23 January 2006

$$I_0(u,v) = \int_0^\alpha t(\theta)\sqrt{\cos\theta}\,\sin\theta(1+\cos\theta)J_0\left(\frac{v\sin\theta}{\sin\alpha}\right)\exp\left(\frac{iu\cos\theta}{\sin^2\alpha}\right)d\theta \tag{3}$$

$$I_1(u,v) = \int_0^\alpha t(\theta)\sqrt{\cos\theta}\,\sin^2\theta J_1\left(\frac{v\sin\theta}{\sin\alpha}\right)\exp\left(\frac{iu\cos\theta}{\sin^2\alpha}\right)d\theta \tag{4}$$

$$I_2(u,v) = \int_0^\alpha t(\theta)\sqrt{\cos\theta}\,\sin\theta(1-\cos\theta)J_2\left(\frac{v\sin\theta}{\sin\alpha}\right)\exp\left(\frac{iu\cos\theta}{\sin^2\alpha}\right)d\theta \tag{5}$$

The AMP spatially modifies the phase of the wave front according to the spatial phase transfer function $t(\theta)$. In applying these formulae, the following approximations are implicit. (1) All inhomogeneous waves are ignored. (2) The Kirchoff boundary conditions are imposed, which is appropriate for AMPs having macroscopic features, as considered here. (3) The Debye approximation is also applied, so only rays falling within the numerical aperture of the lens are considered [25,26]. Note that the electric field distribution along the optical axis, $E(u,v = 0)$, only depends upon $I_0(u,v = 0)$ giving:

$$E(u,v=0) = -iA\int_0^\alpha t(\theta)\sqrt{\cos\theta}\,\sin\theta(1+\cos\theta)\exp\left(\frac{iu\cos\theta}{\sin^2\alpha}\right)d\theta \tag{6}$$

The two- and three-zone AMPs investigated are comprised of a set of N concentric annular zones each having constant differential phase transmittance Φ_i (Fig. 1). The radial extent of the AMP, R, is matched to the limiting aperture of the lens. The radius of the ith zone may be expressed as a dimensionless fraction of R using $r_i = \sin(\theta_i)/\sin(\alpha)$, where θ_i is the aperture half-angle of the ith zone. The optical characteristics of an AMP are determined by the radius and relative phase of each zone. As such, the innermost zone may always be set to $\Phi_1 = 0$, and the others may be varied independently over the interval $[0, 2\pi]$. The number of independent degrees of freedom is then two for a two-zone AMP (r_1 and Φ_2, where $0 < r_1 < 1$), and it is four for a three-zone AMP (r_1, r_2, Φ_2, and Φ_3, where $0 < r_1 < r_2 < 1$).

The two- and four-dimensional solutions spaces associated with a two- and three-zone AMP, respectively, were discretized and the PSF was calculated using Eqs. (1) - (5) for each unique combination of zone radii and relative phases. The solutions space was evaluated using a coarse discretization of $\Delta\Phi = 2\pi/20$ and $\Delta r = 0.05$. Specific regions of interest were studied in greater detail as needed by decreasing $\Delta\Phi$ and Δr. The PSF for each set of AMP parameters was characterized relative to the diffraction limited pattern in terms of (1) the axial (transverse) width of the central lobe; (2) the peak intensity; and (3) the intensity of the largest side lobe(s). The peak in the PSF pattern having the highest intensity was regarded as the central lobe. Under this definition, the central lobe is not necessarily centered at the Gaussian focus. The axial (transverse) extent of the central lobe was quantified using a super-resolution factor, G, defined as the full-width at half-maximum (FWHM) of the central lobe divided by the same in the diffraction limited pattern. The axial Strehl ratio, S, is defined as the peak intensity of the central lobe normalized to that of the diffraction limited pattern. The relative intensity of the largest axial side lobe is quantified using the parameter, M, which is defined as the peak-intensity of the side lobe divided by that of the central lobe.

3. Results and discussion

Figure 3 summarizes the characteristic changes to the axial PSF that result when a two-zone AMP is placed in front of the lens. G, M, and S all exhibit the greatest variation as a function of r_1 along the line $\Phi_2 = \pi$, and the plots are symmetric about this line. G varies from a maximum of 2.31 ($\Phi_2 = \pi$ and $r_1 = 0.54$) to a minimum of 0.90 ($\Phi_2 = \pi$ and $r_1 = 0.76$). Thus, a two-zone AMP could be used to elongate the central lobe by as much as a factor of two.

#10013 - $15.00 USD Received 19 December 2005; revised 21 January 2006; accepted 23 January 2006

Where $G = 0.90$, the axial intensity distribution is comprised of two partly overlapping lobes of equal peak intensity, so $M = 1$. Given that there are two lobes in the intensity distribution, the PSF cannot reasonably be regarded as super-resolved. This finding is consistent with that reported by Sales, who evaluated super-resolution in terms of the separation of minima in the axial PSF in the confocal mode [4]. The absolute intensity of this central lobe pair is reduced relative to the central lobe of the diffraction limit in the amount $S = 0.35$.

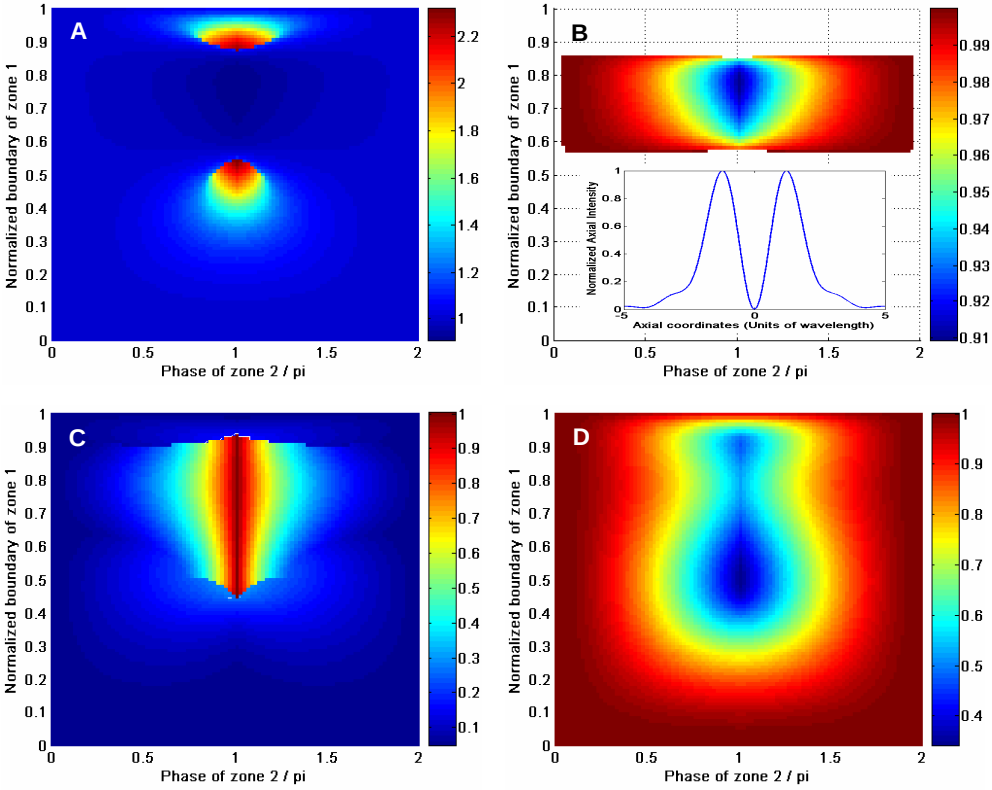

Fig. 3. Characteristic changes to the axial PSF affected by a two-zone AMP. Shown are (**A**) the super-resolution factor G, (**B**) the sub-space of $G < 1$ on an expanded scale, (**C**) the side lobe intensity M, and (**D**) the Strehl ratio S versus $[r_1, \Phi_2]$. The two-dimensional solutions space was discretized by intervals of $\Delta\Phi = 2\pi/100$ and $\Delta r = 0.01$. The inset to B shows the normalized double-peaked axial distribution that results for $r_1 = 0.7$ and $\Phi_2 = \pi$.

Simulations of the PSF over the complete multi-dimensional solutions space for two- and three-zone AMPs both show that the largest variation in G and the greatest super-resolution occurs when successive zones of the AMP differ in phase by π. The overall appearance of the PSF is determined by the vector sum of the electric field component of rays that converge near the focus. The greatest overall variation can be expected then when rays recombine with the highest degree of destructive interference, or when they successively differ in phase by π.

To study the axial super-resolution that can be achieved with a 3-zone AMP in greater detail, the zone phases were fixed to $\Phi_1 = 0$, $\Phi_2 = \pi$, and $\Phi_3 = 0$, and the axial PSF was simulated with the $[r_1, r_2]$ space discretized by $\Delta r = 0.01$. The corresponding plots of G, M, and S versus r_1 and r_2 are shown in Fig. 4. The PSF characteristics are only defined for the upper-left half of the $[r_1, r_2]$ space due to the constraint $0 < r_1 < r_2 < 1$. G takes a minimum value of 0.73 at $r_1 = 0.60$ and $r_2 = 0.77$; however, M is approximately unity under these conditions because the axial intensity distribution near the focus actually consists of three lobes having nearly the same peak intensity. This is similar to the circumstances under which G is minimized for a two-zone AMP.

#10013 - $15.00 USD Received 19 December 2005; revised 21 January 2006; accepted 23 January 2006

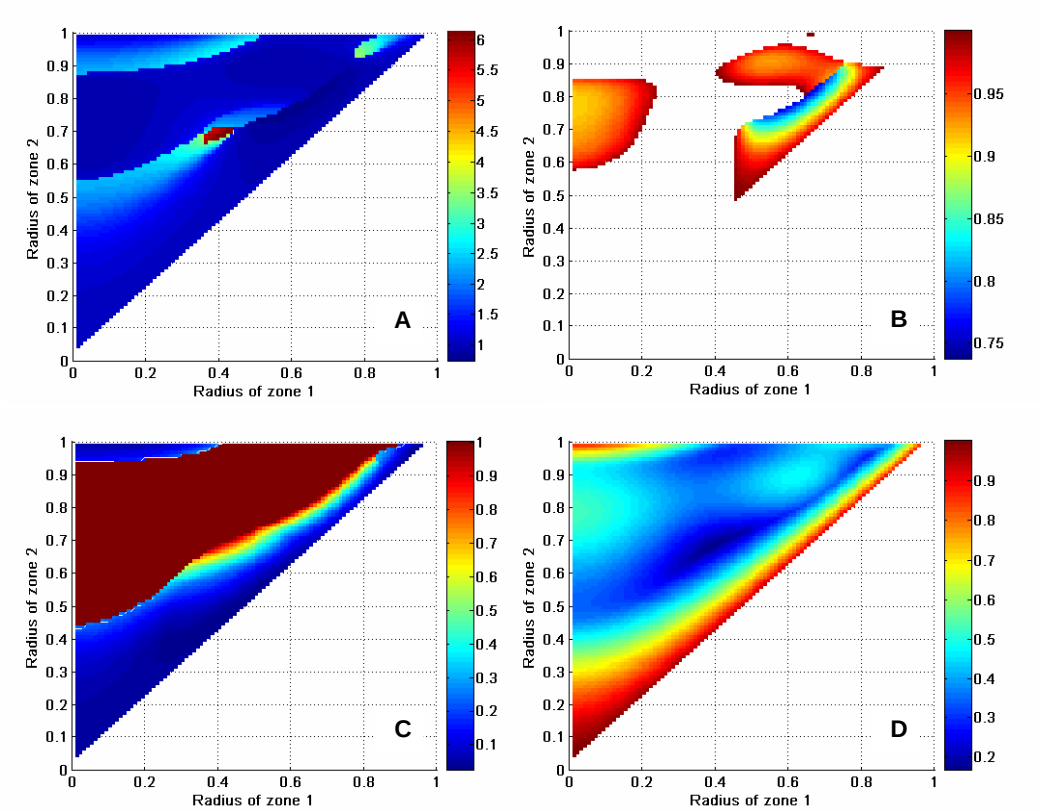

Fig. 4. Characteristic changes to the axial PSF affected by a three-zone AMP having $\Phi_1 = 0$, $\Phi_2 = \pi$, and $\Phi_3 = 0$ as a function of radial zone boundaries r_1 and r_2. Shown are (**A**) the super-resolution factor G, (**B**) the sub-space $G < 1$ on an expanded scale, (**C**) the side lobe intensity M, and (**D**) the Strehl ratio, S. The two-dimensional solutions space $[r_1, r_2]$ was discretized by intervals of $\Delta r = 0.01$.

The vector diffraction calculations show that in general increased axial super-resolution of the central lobe is strongly correlated with a decrease in the Strehl ratio and an increase in the intensity of the side lobes. Similar conclusions have been reported previously for scalar studies of axial super-resolution [3,27]. A similar trade-off is known for changes in the transverse intensity distribution in the focal plane [3,4]. On the basis of conservation of power, the intensity of side lobes in the transverse direction of the focal plane must also increase in those situations for which the axial Strehl ratio is observed to decrease. This implies then that the axial and transverse PSF are coupled, and the axial and transverse spot size cannot be separately engineered. Thus, in designing an AMP the complete 3D PSF must be considered within the context of a given application and with regard for how the photo-activated process depends upon the 3D intensity distribution about the focal region.

To augment this point, let us consider the application of PSF engineering to a photolithographic technique known as three-dimensional microfabrication (3DM). In 3DM, complex microstructures can be fabricated by patterned scanning of a tightly focused pulsed laser beam within the volume of a multi-photon-excitable medium [28]. The structure resolution is determined by the axial and transverse size of the photo-processed volume element or voxel generated at the focus. For most photo-induced processes, the material response to the local intensity is nonlinear (whether one- or multi-photon induced), so the voxel is defined by those points in the PSF for which the local intensity exceeds the photo-response threshold of the medium [28-30]. The average focused power can be adjusted so that a selected isophote matches the threshold intensity. It is practical then to consider the situation that results when the threshold matches the 50% isophote, for which the resulting voxel shape would match the 50% isophote surface. In this case, the axial (transverse) size of

#10013 - $15.00 USD Received 19 December 2005; revised 21 January 2006; accepted 23 January 2006

the voxel as a function of AMP configuration would be given by the axial (transverse) super-resolution factor G, if only the central lobe has appreciable intensity. Note, however, that if the side lobe intensity exceeds 50%, then the photo-processed volume will be comprised by multiple features.

Previous studies of super-resolution have defined the spot-size in terms of the separation between local minima adjacent to the central lobe. Such a definition is appropriate for imaging applications, but poorly suited to lithographic processes (like 3DM) because the minima may or may not correspond to points at which the intensity is zero and they do not alone indicate the shape of the PSF with respect to the photo-response threshold. Clearly, side lobe intensity and the Strehl ratio are relevant when considering the super-resolution that can be achieved in a given application.

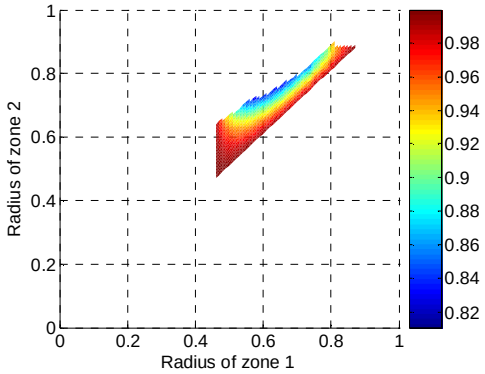

Fig. 5. Sub-space of G versus $[r_1, r_2]$ for a three-zone AMP having $\Phi_1 = 0$, $\Phi_2 = \pi$, and $\Phi_3 = 0$ for which axial super-resolution is achieved ($G < 1$) and side lobe intensity remains below 50% of the peak value ($M < 0.5$).

The super-resolving performance of a three-zone AMP can be evaluated using criteria that account more thoroughly for overall changes in the 3D-PSF. Figure 5 is a plot of axial G for all points in the $[r_1, r_2]$ space for which $G < 1$ and $M < 0.5$. This represents the sub-set of three-zone AMPs that yield an axially super-resolved focus and for which the intensity of the side lobes remains below 50% of the peak intensity. Under these criteria, the maximum axial super-resolution occurs for $r_1 = 0.58$, $r_2 = 0.73$, $\Phi_1 = 0$, $\Phi_2 = \pi$, and $\Phi_3 = 0$, at which point $G = 0.81$, $M = 0.47$, and $S = 0.38$. The effect of this AMP on the 3D-PSF is shown in Fig. 6. The intensity distribution along the optic axis shows clearly that super-resolution is achieved at the expense of higher side lobes. The transverse intensity distribution also shows that some power is re-distributed into weak side lobes, which is consistent with the decrease in the Strehl ratio. This AMP could be used for 3DM, 3D optical data storage/read-out, or any other application that requires a co-minimized axial and transverse intensity distribution and minimized side lobes.

In certain regions of the PSF solutions space, the AMPs elongate the PSF so that the intensity along the optic axis remains high over a greater distance from the focal plane ($G_{axial} > 1$). This can also be viewed as an extended depth of focus. Similar findings have been reported for annular phase DOEs [7,20]. In the case of the two-zone AMP, G_{axial} takes a maximum value of 2.31 at $\phi_2 = \pi$ and $r_1 = 0.54$. Under these conditions the lateral extent of the central lobe is $G_{trans} = 1.00$, as measured in the transverse plane that contains the peak axial intensity. Even greater PSF elongation can be obtained with a three-zone AMP, which produces a maximum value of $G_{axial} = 6.1$ for $r_1 = 0.43$, $r_2 = 0.69$, $\phi_1 = 0$, $\phi_2 = \pi$, and $\phi_3 = 0$. The axial and transverse intensity distribution in the plane of polarization (xz-plane) is shown in Fig. 7. The elongated PSF appears to be the result of close overlap between a focal-plane centered lobe and four adjacent axial side lobes. The outer side lobes of the set attain the same peak intensity as the focal-plane centered lobe, and the intensity between lobes decreases to only ~60% of the peak value. It is noteworthy that the transverse width of the

#10013 - $15.00 USD Received 19 December 2005; revised 21 January 2006; accepted 23 January 2006

central lobe remains nearly invariant along the full length of the five-lobe set (G_{trans} = 0.99 in the Gaussian focal plane). This intensity profile could be used for laser drilling and laser machining applications in which sub-diffraction-limited features are created over an axial distance of several microns. It could also be used in microscopy and imaging applications for achieving sub-diffraction-limited resolution over an extended depth of field.

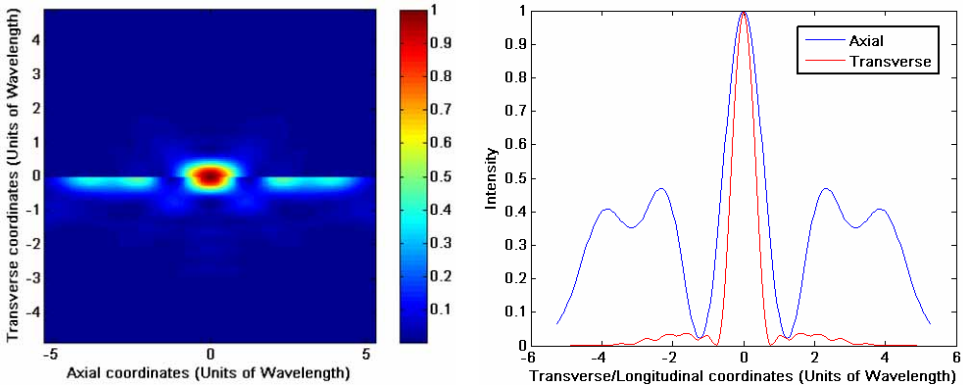

Fig. 6. Comparison of the focused PSF generated when a three-zone AMP having $\Phi_1 = 0$, $\Phi_2 = \pi$, $\Phi_3 = 0$, $r_1 = 0.58$, and $r_2 = 0.73$ is placed before the lens. (**Left-top**) Normalized axial and transverse intensity distribution within the plane of polarization (*xz*-plane) in the diffraction-limit (no AMP) and (**Left-bottom**) when the three-zone AMP is present. (**Right**) Axial and transverse intensity distribution of the AMP-modified beam alone. The AMP-generated PSF is axially super-resolved by $G_{axial} = 0.81$, with $M = 0.47$ and $S = 0.38$, whereas the transverse intensity distribution of the central lobe is minimally broadened by $G_{trans} = 1.01$.

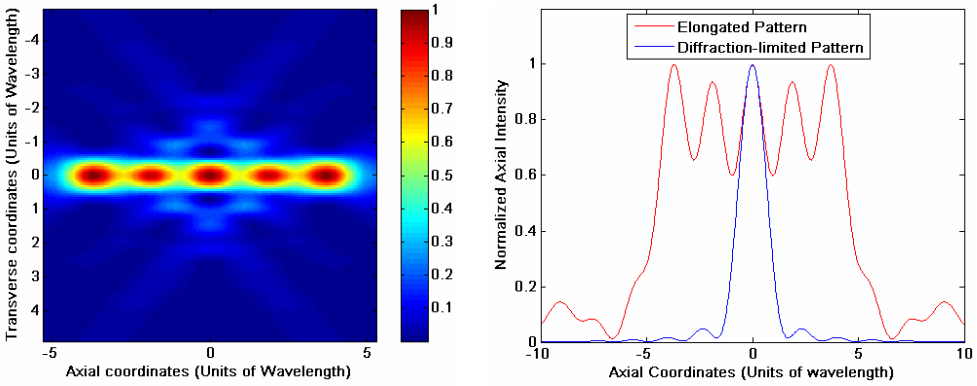

Fig. 7. (**Left**) Normalized axial and transverse intensity distribution in the plane of polarization (*xz*-plane) resulting when a three-zone AMP having $r_1 = 0.43$, $r_2 = 0.69$, $\Phi_1 = 0$, $\Phi_2 = \pi$, and $\Phi_3 = 0$ is placed before the lens. The PSF is axially elongated by a factor of $G_{axial} = 6.1$ yet remains diffraction limited in the transverse direction ($G_{trans} = 0.99$). (**Right**) AMP-modified axial intensity distribution (red trace) versus that computed for diffraction limited focusing (no AMP, blue trace).

The effect of annular DOEs on G_{trans} was considered in some earlier studies of axial super-resolution [17,19,31]. There, it is shown that Eq. (6) expressed in the scalar approximation can be re-written as a one-dimensional Fourier transform of the pupil function *t* through the change of variables $\zeta = [(\cos\theta - \cos\alpha)/(1 - \cos\alpha)] - 0.5$. In these works, centrosymmetric DOEs – those for which $t(\zeta)$ is an even function – are shown to leave $G_{trans} = 1$. However, the subject does not appear to have been explored to a level that one may conclude $G_{trans} = 1$ *if and only if* the DOE is centrosymmetric. We note that the DOEs discussed in the present work are not exclusively centrosymmetric (*e.g.* the AMPs corresponding to Figs. 6 and 7 are

#10013 - $15.00 USD Received 19 December 2005; revised 21 January 2006; accepted 23 January 2006

non-centrosymmetric). These results suggest that minimal change to the transverse PSF can also be achieved with certain non-centrosymmetric DOE configurations.

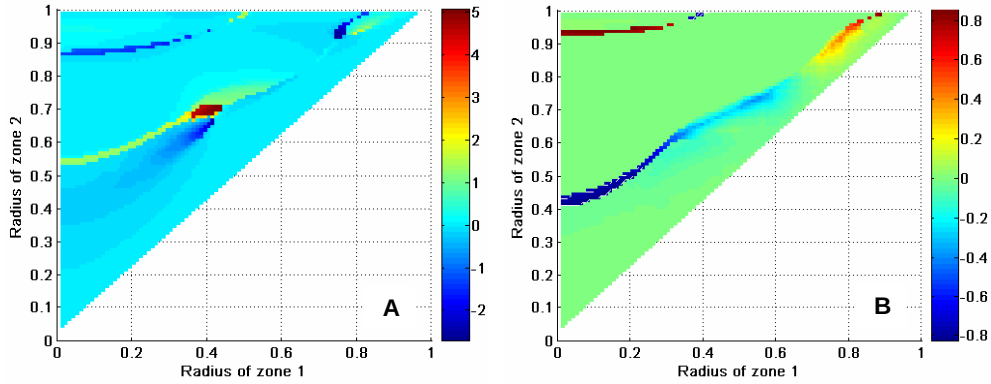

Fig. 8. Comparison of the axial PSF parameters G and M as calculated using vector diffraction and scalar theory for three-zone AMPs having $\Phi_1 = 0$, $\Phi_2 = \pi$, and $\Phi_3 = 0$. (**A**) G_{vector} - G_{scalar} and (**B**) M_{vector} - M_{scalar} versus $[r_1, r_2]$.

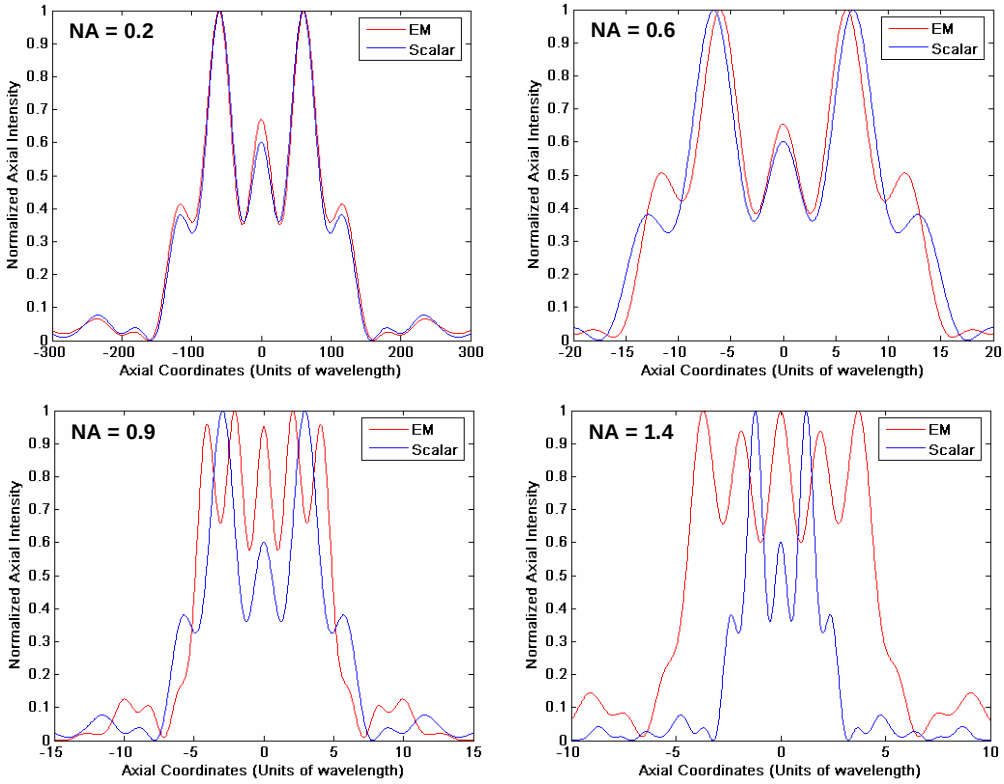

Fig. 9. Comparison of the normalized axial intensity distribution in the plane of polarization (xz-plane) calculated using vector diffraction (EM) and scalar theory at four values of NA for the case in which a three-zone AMP having $r_1 = 0.43$, $r_2 = 0.69$, $\Phi_1 = 0$, $\Phi_2 = \pi$, and $\Phi_3 = 0$ is placed before the lens.

Although it is commonly agreed that high-NA focal field distributions are not accurately described by scalar theory or methods that employ the paraxial approximation, the magnitude of the discrepancy has not been widely examined. This subject was investigated

#10013 - $15.00 USD Received 19 December 2005; revised 21 January 2006; accepted 23 January 2006

quantitatively by using both vector diffraction and scalar theory [4] to compute axial PSFs generated with three-zone AMPs having $\Phi_1 = \Phi_3 = 0$ and $\Phi_2 = \pi$ and then plotting the differences in the characteristic parameters $G_{vector} - G_{scalar}$ and $M_{vector} - M_{scalar}$ versus $[r_1, r_2]$ (Fig. 8). It was found that both levels of theory predict *qualitatively* similar changes in the PSF as a function of AMP configuration and the values of the characteristic PSF parameters G and M are similar. Yet they differ most in those situations for which the PSF undergoes extreme axial change, be that super-resolution or elongation (compare Figs. 8 and 4). To illustrate the point further, Fig. 9 shows the evolution of the axial intensity distributions calculated using the vector diffraction and scalar methods at four values of NA for a three-zone AMP having $r_1 = 0.43$, $r_2 = 0.69$, $\Phi_1 = 0$, $\Phi_2 = \pi$, and $\Phi_3 = 0$, which produces the axially stretched PSF shown in Fig. 7 (at $NA = 1.4$). Although both levels of theory predict that the PSF is axially elongated, the patterns differ significantly as the NA increases. Notably, we find that $G_{vector} - G_{scalar} = 5.04$ at $NA = 1.4$. Thus, scalar theory may be useful for rapid, qualitative assessment of DOEs under high-NA conditions, but vector diffraction theory appears essential for accurate simulation of the PSF.

4. Conclusion

Vector diffraction theory was used to examine the effect of two- and three-zone AMPs on the 3D-PSF generated under high-NA focusing of linearly polarized incident light. A systematic approach was adopted in which PSFs were calculated and compared for all possible combinations of phase and zone radius within the discretized two- and four-dimensional space associated with two- and three-zone AMPs, respectively. Two-zone AMP configurations were identified that marginally decrease the axial width of the central lobe, but this is accompanied by a large increase in the intensity of adjacent side lobes that make the achievable intensity distributions unsatisfactory for most applications. Conditions were found for which a three-zone AMP yields an axial intensity distribution that is super-resolved by 19% with minimal change in the transverse profile and sufficiently small side lobes that the intensity pattern could be used for micro-lithographic and micro-imaging applications. Interestingly, conditions were also identified for which the axial PSF is elongated by 510% with only 1% change along the transverse direction. This intensity distribution could be used for sub-micron-scale laser drilling and machining. A comparison of intensity distributions calculated under high-NA conditions using vector and scalar theories shows that the latter is suitable for identifying qualitative changes in the PSF, but the detailed intensity distribution can differ markedly from that computed using the more accurate vector diffraction method.

Acknowledgements

The authors would like to thank the reviewers for their very helpful and constructive comments.

#10013 - $15.00 USD Received 19 December 2005; revised 21 January 2006; accepted 23 January 2006